Low Effective Activation Energies for Oxygen Release from Metal Oxides: Evidence for Mass-Transfer Limits at High Heating Rates

Guoqiang Jian, Lei Zhou, Nicholas W. Piekiel, and Michael R. Zachariah*[a]

Oxygen release from metal oxides at high temperatures is relevant to many thermally activated chemical processes, including chemical-looping combustion, solar thermochemical cycles and energetic thermite reactions. In this study, we evaluated the thermal decomposition of nanosized metal oxides under rapid heating ($\sim 10^5$ K s^{-1}) with time-resolved mass spectrometry. We found that the effective activation-energy values that were obtained using the Flynn–Wall–Ozawa isoconversional method are much lower than the values found at low heating rates, indicating that oxygen transport might be rate-determining at a high heating rate.

1. Introduction

Metal oxides are employed as oxygen carriers in chemical-looping combustion,[1] thermite reactions,[2] and as part of a redox couple in solar thermochemical fuels production.[3] Central to each of the above applications is oxygen storage and release kinetics at high heating rates. Although extensive work has been carried out on the decomposition kinetics of solid systems,[4,5] very few studies of decomposition kinetics of metal oxides at high heating rates have been reported. The primary reason could be that traditionally, quantitative measurements of the solid-state reaction kinetics are usually performed using commercial thermal analysis techniques at low heating rates,[4,5] which fail in the measurement of rapid chemical processes. Recently, the use of metal oxides as oxygen carriers in combustion/explosion reactions[2] has motivated researchers to study metal oxide decomposition at high heating-rate conditions closer to those of real-time combustion events. For such investigations, a temperature-jump time-of-flight mass spectrometry (T-jump TOFMS) system was developed based on coupling a mass spectrometer with a pulse-heating temperature-jump probe, which enables one to characterize the chemical transformations under rapid-heating conditions of up to $\sim 10^6$ K s^{-1} in a time-resolved manner.[6] The T-jump TOFMS system has been used to study the decomposition of nitrocellulose and RDX, as well as nanothermite reactions.[6–9] It was found that for some cases, oxygen release from the metal oxide nanoparticle oxidizer might be closely related to the reactivity of nanothermites.[7]

In contrast to the kinetic parameters obtained from traditional thermal analysis techniques (usually mass loss), the T-jump TOFMS system measures the temporal behavior of product species under high heating-rate conditions, which can then be used to determine the overall activation energy based on an isoconversional approach. Vyazovkin et al.[10] have demonstrated that effective activation energies can be derived using mass spectrometry by measuring the species produced in a heating process. White et al.[11–14] calculated the species-specific isoconversion effective activation energies, and showed that species-specific thermal analysis provides information of a specific thermal process, which might be useful for the analysis of complex reaction processes.

In this paper, we describe a new approach to calculate the effective activation energies of nanosized metal oxide decomposition under rapid heating by measuring the chemical species produced using T-jump TOFMS (Figure 1). The effective activation energies obtained using the Flynn–Wall–Ozawa
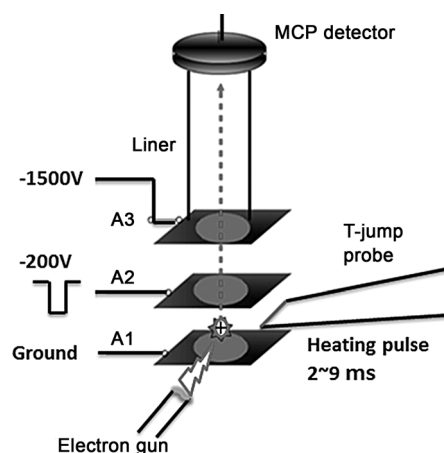
[a] G. Jian, Dr. L. Zhou, Dr. N. W. Piekiel, Dr. M. R. Zachariah
Department of Chemical and Biomolecular Engineering
and Department of Chemistry and Biochemistry
University of Maryland, College Park
MD 20742 (USA)
E-mail: mrz@umd.edu

Supporting Information for this article is available on the WWW under http://dx.doi.org/10.1002/cphc.201301148.

Figure 1. The T-jump TOFMS system. A1: Ion repeller plate, A2: ion extraction plate, A3: ion acceleration plate, and MCP: Microchannel plate detector.

method are also compared with activation energies obtained at lower heating rates. Effective activation energies were found to be much lower than those reported that were obtained using low heating rates, demonstrating the possible presence of mass transfer limitation during reactions at high heating rates. The diffusional effects on the decomposition of nano-sized metal oxides at high heating rates were analyzed.

2. Results and Discussion

2.1. Oxygen Release from Nanosized Metal Oxides Measured Using Temperature-Jump Mass Spectrometry

Time-resolved mass spectra obtained after rapid heating of CuO nanoparticles are shown in Figure 2. In this experiment, the heating duration was about 2.1 ms with a heating rate of
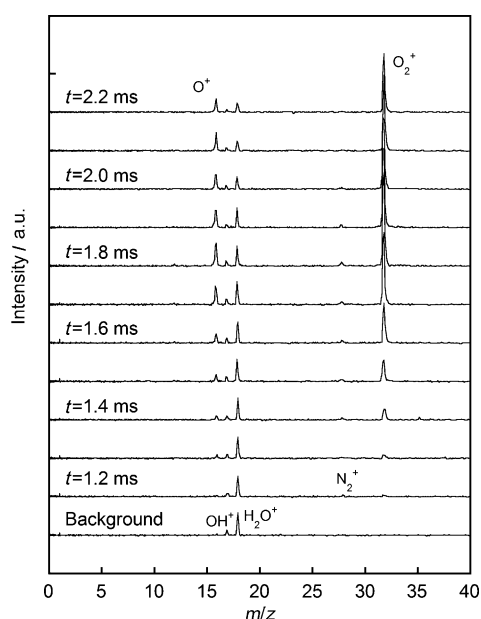
Figure 3. Temporal profile of oxygen release upon rapid heating of CuO nanoparticles at a heating rate of ~6×10^5 K s^{-1}.

to its initial value but remains relatively high for a couple of milliseconds.

Variable heating rate experiments using the same conditions were performed to study the decomposition kinetics at heating rates from ~1.5×10^5 to ~6.5×10^5 K s^{-1}, which enabled us to extract the onset temperature of oxygen release, as shown in Figure 4.

Figure 2. Time-resolved mass spectra of CuO nanoparticle decomposition at a heating rate of ~6×10^5 K s^{-1}.

Figure 4. Oxygen-release temperatures from CuO nanoparticles as a function of the heating rate. Error bars represent the standard deviation caused by the noise in resistance measurement (± 10 K).

~6×10^5 K s^{-1}. We plot the mass spectra obtained between 1.0–2.2 ms in Figure 2, and a background spectrum taken at $t = 0$ ms is also shown. As seen in Figure 2, a strong peak of $m/z = 18$ (H$_2$O) and smaller peaks at m/z of 17 (OH), 28 (N$_2$), are from background species. Mass spectra taken at $t = 1.2$–2.2 ms clearly show oxygen ($m/z = 16$, 32) produced upon rapid heating, and the intensities of these peaks increase with increasing temperature. The temporal behavior of O$_2$ release from CuO nanoparticles is presented in Figure 3 and shows that the onset temperature of O$_2$ release is ~1020 K at a heating rate of ~6×10^5 K s^{-1}. Figure 3 shows that the oxygen intensity increases quickly upon heating and reaches a peak value, after which it starts to decrease again. Because the full release of oxygen from CuO nanoparticles could significantly increase the background pressure level, the oxygen intensity does not go back
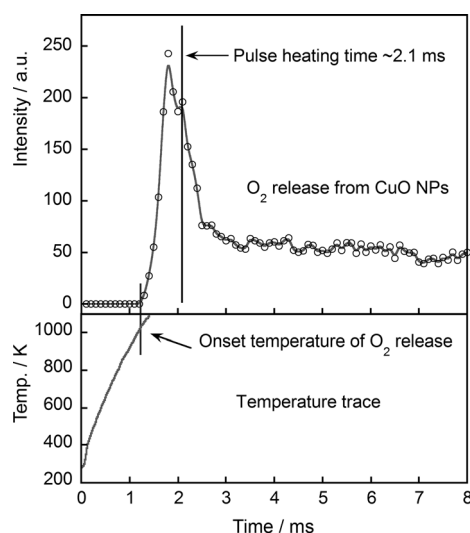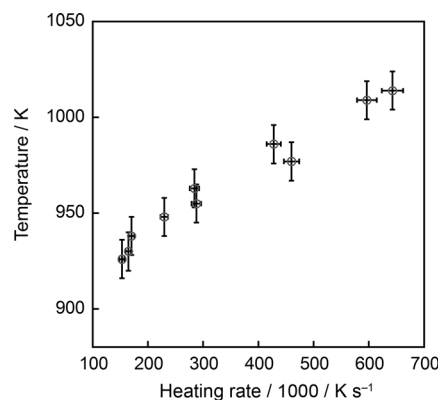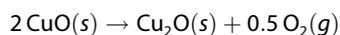
2.2. Activation Energy of Oxygen Release from Nanosized Metal Oxides at High Heating Rates

Similar experiments were also conducted for Fe$_2$O$_3$ and Co$_3$O$_4$ nanoparticles. Because the decomposition of metal oxides at high temperature produces a suboxide and oxygen gas:

$$2\,CuO(s) \rightarrow Cu_2O(s) + 0.5\,O_2(g)$$

the measured oxygen evolution was used to evaluate effective activation energies (E_a). E_a values were calculated from species-

specific intensity versus temperature profiles using the Flynn–Wall–Ozawa method.[15–17] This isoconversion method is based on the principle that the reaction rate at constant extent of conversion is a function of only the temperature, which allows for model-free estimates of the activation energy.

Based on the single-step kinetics derived from the Arrhenius equation, we get Equation (1):

$$\frac{d\alpha}{dt} = A\exp\left(-E_a/RT\right)f(\alpha) \tag{1}$$

Here, the subscript α is a given value of conversion, A is the pre-exponential frequency factor, R is the gas constant, T is the temperature, $f(\alpha)$ is the reaction model in terms of conversion, and E_a is the activation energy.[18] Following the isoconversion principle, the kinetics of the solid-sample reactions can be described as shown in Equation (2):

$$\left[\frac{d\ln\left(d\alpha/dt\right)}{dT^{-1}}\right]_\alpha = -E_a/R \tag{2}$$

For non-isothermal conditions at a constant heating rate β, integration of Equation (1) will involve solving the temperature integral $I(E_a, T)$ [Eq. (3)]:

$$g(\alpha) \equiv A/\beta \int_0^{T_\alpha} \exp\left(-E_a/RT\right)dT = A/\beta I(E_a, T) \tag{3}$$

where $g(\alpha)$ is the integral form of the reaction model. By using Doyle's linear approximation,[19] one arrives at the Flynn–Wall–Ozawa isoconversion method [Eq. (4)]:

$$\ln(\beta) = \text{const.} - 1.05\, E_a/RT_\alpha \tag{4}$$

The isoconversion method is often employed because it does not require an a priori presumption of the reaction model to extract activation energies.[4,5]

Detailed information regarding the interpretation and procedures of using isoconversion methods can be found in a series of publications by Vyazovkin et al.[4,5,18]

As shown in Figures 3 and, the O2-release profile can be obtained for different heating rates. For the kinetic analysis using the Flynn–Wall–Ozawa method, the effective activation energy is dependent on the extent of conversion, and varies in some complex systems with the degree of transformation in a manner that reflects the contributions of indi-

vidual processes. However, we used T-jump TOFMS for identifying the activation energy at the initial stage of metal oxide decomposition, by setting the onset temperature of O2 release as the isoconversion point. The effective activation energy obtained at the initial stage of metal oxide decomposition is not complicated by further decomposition of suboxide to pure metal and oxygen which requires much higher temperature in nonreducing environments (e.g. $2\,Cu_2O \rightarrow 4\,Cu + O_2$).[20,21]

By applying Equation (4), the effective activation energies can be determined from the slope of the Arrhenius plot in Figure 5. The metal oxide nanoparticles demonstrate an acceptable degree of linearity with a correlation coefficient R of 0.96. The effective activation energies calculated from the temperature profile of the O2-ion signal (m/z 32) are 125 ± 17, 144 ± 32, and 77 ± 6 kJ mol^{-1} for CuO, Fe$_2$O$_3$, and Co$_3$O$_4$ nanoparticles, respectively. Uncertainties were estimated based on the linear-regression slope error calculated from a linear fit (Figure 5) with 95% confidence boundaries.

Our experiments, which were conducted in high vacuum, directly probed the decomposition of the metal–oxygen complex within a nanoparticle at high heating rate, and the subsequent escape of molecular oxygen or a volatile metal suboxide.

Although most reported experiments have focused on the kinetic study of metal oxides reacting with reducing reagents (e.g. carbon, hydrogen),[22–25] there are some values of activation energies for direct metal oxide decomposition at low heating rates that have been published. Chadda et al. reported an activation energy for CuO decomposition in air at low heating rate of ~313 kJ mol^{-1}.[26] A value of ~238 kJ mol^{-1} was reported for CuO decomposition in argon.[27] For Co$_3$O$_4$ decomposition, the activation energy was reported to be
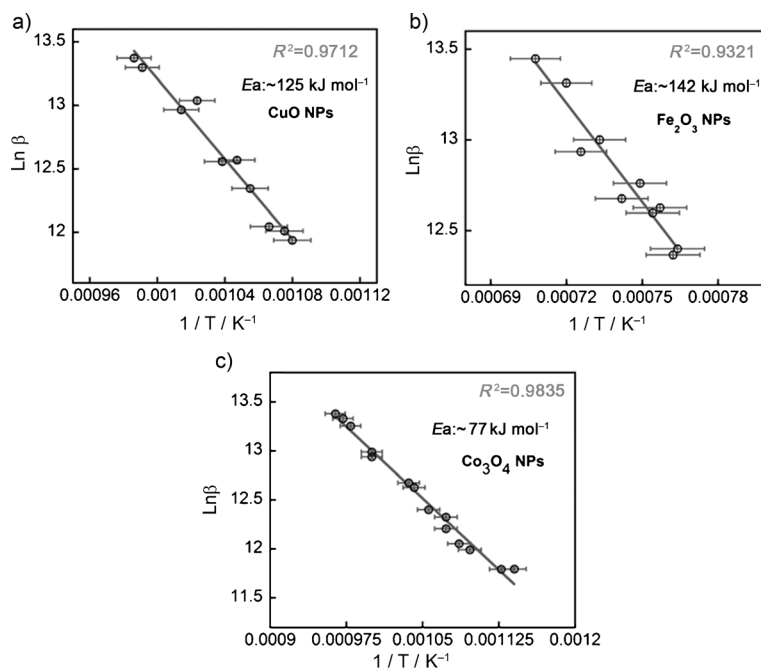

Figure 5. Natural logarithm of the heating rate versus the reciprocal absolute temperature for onset of oxygen release from decomposition of metal oxide nanoparticles (NPs). a) CuO, b) Fe$_2$O$_3$, and c) Co$_3$O$_4$.

~293 kJ mol^{-1} in argon.[27] Later, Malecki et al. reported a E_a value of ~153 and 164 kJ mol^{-1} for Co$_3$O$_4$ powder and single crystal in a partial vacuum (oxygen partial pressure ~0.67 Pa).[28] As far as we are aware, no activation energy of direct Fe$_2$O$_3$ decomposition has been reported, possibly because of the high decomposition temperature of Fe$_2$O$_3$ which hindered the use of traditional thermal analysis to obtain kinetics parameters.

The previously reported activation energies are all for microsized metal oxide particles. To address this point, we ran low heating rates kinetics measurements for metal oxides nanoparticles in a thermogravimetric analysis (TGA) using the same isoconversion approach. The activation energies for the initial decomposition were found to be 191, 334, and 269 kJ mol^{-1} for CuO, Fe$_2$O$_3$, and Co$_3$O$_4$ nanoparticles, respectively. Apparently, the activation energies at low heating rates are much higher than those values obtained at high heating rates, as compiled in Table 1. In addition, we did not notice any significant reduction in the activation energies of nanosized metal oxides, compared to the reported values of microsized particles under low heating rates.

Table 1. Effective activation energies measured by the isoconversional method at low and high heating rates.

Methods	Metal oxide nanoparticles	CuO	Fe$_2$O$_3$	Co$_3$O$_4$
[a]	E_a [kJ mol^{-1}]	191	334	269
[b]	E_a [kJ mol^{-1}]	125	142	77

[a] Low heating rates in TGA based on a 10% conversion. [b] High heating rates in T-jump.

For condensed-phase kinetics studied using the isoconversion method, the measured effective activation energies can reflect several factors, such as surface properties of the solid, diffusion effects of products and/or reactants, and the reducing environment.[23,29,30] In particular, two primary factors could contribute to the observed lower effective activation energies: size effects, and high heating rates. It has been reported that kinetic parameters could change as the particle size decreases to the nanometer scale. Yue et al.[31] found a decrease in the effective activation energy of up to 70–80 kJ mol^{-1} for the decomposition of nanosized calcite. Reduction of the activation energy was also found for nanoscale metal oxidation.[32] This has been attributed to the excessive surface energies of nanoparticles. Navrotsky et al.[33,34] have studied the stability of metal oxide systems at the nanoscale, and found that nanophase metal oxides show large thermodynamically driven shifts in the oxidation–reduction equilibria. Based on the available surface enthalpy data for iron oxide and cobalt oxide systems,[33,34] we estimated that the contribution of the surface enthalpy of ~50 nm nanoparticles to the total reaction enthalpy is less than ~5%, indicating that size effects do not lead to a significant lowering of the observed activation energy.

Indeed our measured activation energies for metal oxide nanoparticles (Table 1) at low heating rates are not significantly

different from those reported for microsized particles. We attribute the lower activation energies to the high heating rates used, which is consistent with the results obtained by high heating rate micro-differential scanning calorimetry,[35] also showing lower activation energies at high heating rates. Similar lower activation energies at high heating rates were also reported by other groups for, for example, thin-film samples and biomass, though the heating rates used were lower than ours.[36–38]

It is not unreasonable to assume that at some level of heating rate the observed reaction rate is constrained by the oxygen transport within the material.

In their review paper, Malinin and Tolmachev[27] summarized two different types of metal oxide decomposition pathways. Type 1 produces both atomic and molecular oxygen, whereas type 2 involves only molecular oxygen in the decomposition (e.g. Ag$_2$O→Ag).[27,39] Available experimental data indicate that the processes CuO→Cu$_2$O and Co$_3$O$_4$→CoO release both atomic and molecular oxygen and thus belong to the first type. The reaction Fe$_2$O$_3$→Fe$_3$O$_4$ has also been found to produce both oxygen atoms and molecules.[39,40] Therefore, all three metal oxides in this study belong to type 1, which produces both atomic and molecular oxygen. The generally accepted scheme for the type 1 decomposition is:[27,39]

1) O^{2-} (lattice) → 2 e + O (surface)

2) 2 O (surface) → O$_2$ (adsorbed) → O$_2$(g) or
   2 O (surface) → 2 O(g)

3) Formation and growth of nuclei of a new phase.

Because all the materials studied in this work fall into the type 1 category, we use the example of CuO. The decomposition of CuO is known to afford a dense product, as revealed by in situ transmission electron microscopy (TEM)[41,42] and scanning electron microscopy (SEM) experiments.[43] This is possibly because the initial volume of CuO does not greatly differ from the oxide products[27] (the density of CuO and Cu$_2$O is 6.3 and 6.0 g cm^{-3}, respectively). Therefore, the oxygen formed in the phase boundary should either diffuse out through the bulk or grain boundary of Cu$_2$O, as shown in Figure 6 b. Perinet et al. systematically studied the oxygen diffusion in Cu$_2$O by an ^{18}O-tracer technique, and reports that neutral interstitial oxygen is responsible for the diffusion in both grain boundaries and the bulk.[44] Ideally, the decomposition process proceeds similar to
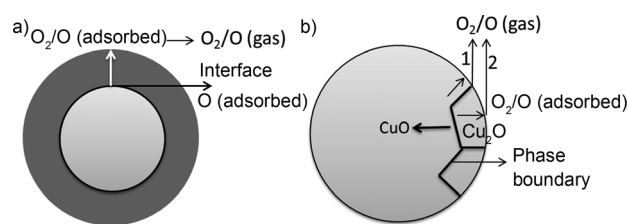

Figure 6. Models for CuO nanoparticle decomposition. a) Shrinking-core model, and b) boundary-diffusion model; note: two possible paths of phase-boundary diffusion (1) and bulk diffusion (2).

a shrinking-core model, as shown in Figure 6a. However, it is more likely to proceed through a phase-boundary-moving process shown in Figure 6b as boundary-diffusion processes have a much lower energy barrier. In an in situ TEM study of CuO reduction to Cu_2O in a vacuum, Li et al. found that grain boundaries provide easy paths for oxygen release, with an activation energy of ~ 106 kJ mol^{-1}.[41,42] They estimated a diffusion coefficient of $\sim 10^{-9}$–10^{-10} cm^{2}s^{-1} (at ~ 1000 K) for oxygen diffusion in Cu_2O grain boundaries,[45] which is higher than the $\sim 10^{-11}$–10^{-12} cm^{2}s^{-1} value obtained for bulk Cu_2O.[44,45]

If we propose, as in Figure 6b, that oxygen diffusion occurs along the Cu_2O grain boundaries, and is the rate-limiting step in oxygen release at high heating rates, we can test this hypothesis by estimating the diffusion time (t_d) for oxygen through the phase boundary with a simple scaling analysis, $t_d \approx L^2/D$, where D is the grain boundary diffusion coefficient $\sim 10^{-9}$–10^{-10} cm^{2}s^{-1}, and L is the particle radius ~ 25 nm. This yields timescales on the order of milliseconds (~ 6–60 ms), which is consistent with the timescales we observed in our mass spectra.

If we continue our assumption, based on the work of Li et al.[41,42] that transport is primarily through the phase boundary, we can liken this to reaction/diffusion problems that have been previously investigated for reactions within catalyst particles.[46] Borrowing directly from that analysis, one can define the effectiveness factor η, as the observed reaction rate divided by the intrinsic reaction rate [Eq. (5)]:

$$R_{obs} = k_{obs}f(c) = \eta k f(c) = \eta A e^{-\frac{E_a}{RT}} f(c) \tag{5}$$

where R_{obs} is the observed reaction rate, $f(c)$ is a function of reactants concentration, and dependent on the reactant concentration, k is the intrinsic reaction rate constant, A is a pre-exponential factor, and E_a is the intrinsic chemical activation energy.

In the limit of low effectiveness factors η (internal-diffusion-controlled) is [Eq. (6)]:

$$\eta \propto h_T \tag{6}$$

where h_T is the Thiele modulus, the square of which is proportional to the ratio of the reaction to diffusion. Based on its definition, we obtain Equation (7):

$$h_T \propto \sqrt{\frac{k}{D_c}} \tag{7}$$

where D_c is the diffusivity of oxygen species. From Equations (5)–(7), we obtain Equation (8):

$$k_{obs} \propto \frac{k}{\sqrt{\frac{k}{D_c}}} = \sqrt{kD_c} \tag{8}$$

Diffusivity D_c (oxygen diffusivity in the phase boundary) can be written as Equation (9):[47]

$$D_c = A_d e^{-\frac{E_d}{RT}} \tag{9}$$

where A_d is a temperature-independent quantity and E_d is the activation energy of the diffusion process; this leads us to Equations (10) and (11):

$$k_{obs} \propto \sqrt{kD_c} = \sqrt{\left(A e^{-\frac{E_a}{RT}}\right)\left(A_d e^{-\frac{E_d}{RT}}\right)}$$
$$= A^{1/2} \times A_d^{1/2} e^{-\frac{(E_a + E_d)}{2RT}} \tag{10}$$

$$E_{eff} = \frac{(E_a + E_d)}{2} \sim \frac{E_a}{2} \tag{11}$$

From Equation (11), the effective activation energy E_{eff} is half the intrinsic chemical activation energy.

The result of Equation (11) can is also obtained by an alternative approach. Equation (5) can be further expressed as Equation (12):

$$\ln R_{obs} = \ln \eta k_0 - \frac{E_a}{RT} + \ln f(c) \tag{12}$$

so that [Eq. (13)]:

$$\frac{d\{\ln(R_{obs})\}}{d(1/T)} = -\frac{E_a}{R} + \frac{d\{\ln(\eta)\}d\{\ln(h_T)\}}{d\{\ln(h_T)\}d\ln(1/T)} \tag{13}$$

At constant diffusion coefficient [Eq. (14)]:

$$\frac{d\{\ln(h_T)\}}{d(1/T)} = -\frac{E_a}{2R} \tag{14}$$

we obtain Equation (15):

$$-\frac{E_{eff}}{R} = -\frac{E_a}{R}\left[1 + \frac{1}{2}\frac{d\{\ln(\eta)\}}{d\{\ln(h_T)\}}\right] \tag{15}$$

For kinetic-control reactions, small values of h_T, $d\{\ln(\eta)\}/d\{\ln(h_T)\} \approx 0$, imply that $E_{eff} = E_a$, whereas for large values of h_T (i.e. internal transport control), $d\{\ln(\eta)\}/d\{\ln(h_T)\} \approx -1$, we obtain $E_{eff} = E_a/2$.

From both Equations (11) and (15), it can be seen that within the limit of transport control the effective activation energy E_{eff} reduces to half the intrinsic chemical activation energy.

In other words, at high heating rates, oxygen donation from oxygen carriers is limited by condensed-state transport processes.

3. Conclusion

We used T-jump TOFMS to study the kinetics of decomposition for three metal oxide nanoparticles (CuO, Fe_2O_3, and Co_3O_4) at heating rates of $\sim 10^5$ K s^{-1}. The isoconversion effective activation energies were calculated based on the time-resolved mass spectra information and temperature profiles, and were found to be significantly lower than activation energies at slow heat-

ing rates. The lower activation energies obtained at high heating rates in this study imply that even for nanoparticles which have small diffusional length scales, high heating rates can result in a situation where mass-transfer constraints are observed. This should have implications for how systems that use metal oxides as oxygen carriers are selected. The results also imply that the choice of oxygen carrier/donor should not be made simply on the basis of thermochemical constraints.

Experimental Section

Materials

The samples used in this study included CuO, Fe_2O_3, and Co_3O_4 nanoparticles, all of which were obtained from Sigma–Aldrich, were designated as < 50 nm by the supplier. TEM (JEOL 2100F, Tokyo, Japan) analysis show that the primary particle-size distribution is around 30–50 nm; some particles larger than 50 nm also exist in the sample (see the Supporting Information).

High-Heating-Rate Kinetics Measurement

The fast-heating experiments were conducted in a self-designed temperature-jump time-of-flight mass spectrometer at heating rates ranging from ~1 to 7×10^5 Ks^{-1}. A drawing of the T-jump TOFMS system is shown in Figure 1. The instrument is comprised of a linear time-of-flight chamber, an electron gun ionization source, a T-jump probe with a Pt filament for sample heating, and an in-house-built power source to supply a tunable current pulse for rapid heating. The filament was inserted within the ion-extraction zone of the TOF mass spectrometer, which has a background pressure of ~10^{-6} torr. A detailed description of the instrument and its operating procedures can be found in our previous publications.[6] The advantage of this T-jump TOFMS system is its capability of achieving simultaneous measurement of species evolution and temperature. There is effectively no time delay between the T-jump heating probe and the mass spectrometer owing to the fact that the T-jump probe is closely located to the ionization zone as shown in Figure 1. The product species are directly produced under high vacuum in a non-collisional environment and are transported to the micro-channel plate detector in less than ~10 µs. In brief, mass spectra were continuously recorded at a temporal resolution of 100 µs, while voltage and current data from the heating pulse were recorded simultaneously. By varying the duration of heating pulse from ~2 to 9 ms, heating rates could be changed in a range of ~$1–7\times10^5$ Ks^{-1}. A new Pt wire was employed for each experimental run. From the recorded voltage and current trace, the temporal temperature history can be found as a function of wire resistance using the well-known Callender–van Dusen equation [Eq. (16)]:[48]

$$R_T = R_0(1 + A*T + B*T^2) \qquad (16)$$

A and B are constants, and R_0 and R_T are the resistance at 0 °C and at T °C, respectively. At higher temperatures (> 1100 K), the temperature of the Pt wire was calibrated using a NIST-calibrated blackbody source (Mikron M350) based on two-color pyrometry centered on 970 and 1550 nm. An extrapolation of the calibration up to 1700 K was performed based on the Sakuma–Hattori equation.[49] Time-resolved mass spectra combined with temperature information were then used for characterization of the metal oxide decomposition at high heating rates.

Prior to heating, the metal oxide nanoparticles were ultrasonicated for 20 min in hexane. The prepared sample suspensions were coated on the central region of the T-jump probe (length ~12 mm, diameter ~76 µm) with a pipette. A dense sample coating was formed after hexane evaporation. The mass of the coating materials on the wire was estimated to be ~90 µg by a high-precision balance (readability $d = 0.001$ mg). A heat-transfer analysis based on a simplified model developed by Ward et al.[50] was carried out to estimate the particle temperature, which indicated that the temperature difference, based on the small thermal contact resistance between nanoparticle and wire, was < 5 K.[51]

Low-Heating-Rate Kinetics Measurement

The slow-heating experiments were conducted in a TGA system (SDT Q600, TA Instruments, USA) under Ar flow (flow rate 50 mL min^{-1}). For each run, ~5 mg of sample was placed inside an alumina crucible pan and heated to the set temperature (1273 K for CuO, 1373 K for Co_3O_4, and 1573 K for Fe_2O_3) in an Ar atmosphere. Thermal analysis experiments for each sample were performed at heating rates of 5, 10, 15, 20, and 30 K min^{-1}.

[1] P. Cho, T. Mattisson, A. Lyngfelt, *Fuel* **2004**, *83*, 1215–1225.
[2] E. L. Dreizin, *Prog. Energy Combust. Sci.* **2009**, *35*, 141–167.
[3] A. Steinfeld, *Sol. Energy* **2005**, *78*, 603–615.
[4] S. Vyazovkin, C. A. Wight, *Annu. Rev. Phys. Chem.* **1997**, *48*, 125–149.
[5] S. Vyazovkin, *Int. Rev. Phys. Chem.* **2000**, *19*, 45–60.
[6] L. Zhou, N. Piekiel, S. Chowdhury, M. R. Zachariah, *Rapid Commun. Mass Spectrom.* **2009**, *23*, 194–202.
[7] L. Zhou, N. Piekiel, S. Chowdhury, M. R. Zachariah, *J. Phys. Chem. C* **2010**, *114*, 14269–14275.
[8] G. Q. Jian, N. Piekiel, M. R. Zachariah, *J. Phys. Chem. C* **2012**, *116*, 26881–26887.
[9] G. Q. Jian, S. Chowdhury, K. Sullivan, M. R. Zachariah, *Combust. Flame* **2013**, *160*, 432–437.
[10] S. Vyazovkin, V. Goryachko, V. Bogdanova, V. Guslev, *Thermochim. Acta* **1993**, *215*, 325–328.
[11] E. Bonnet, R. L. White, *Thermochim. Acta* **1998**, *311*, 81–86.
[12] D. R. White, R. L. White, *J. Appl. Polym. Sci.* **2005**, *95*, 351–357.
[13] R. L. White, *Int. J. Mass Spectrom.* **2009**, *287*, 128–133.
[14] D. R. White, R. L. White, *Appl. Spectrosc.* **2008**, *62*, 116–120.
[15] T. Ozawa, *Bull. Chem. Soc. Jpn.* **1965**, *38*, 1881–1886.
[16] H. Flynn, L. A. Wall, *J. Res. Natl. Bur. Stand.* **1966**, *70*, 487–523.
[17] T. Ozawa, *Thermochim. Acta* **1992**, *203*, 159–165.
[18] S. Vyazovkin, N. Sbirrazzuoli, *Macromol. Rapid Commun.* **2006**, *27*, 1515–1532.
[19] C. D. Doyle, *J. Appl. Polym. Sci.* **1962**, *6*, 639–642.
[20] H. S. Roberts, F. H. Smyth, *J. Am. Chem. Soc.* **1921**, *43*, 1061–1079.
[21] V. V. Galvita, H. Poelman, G. Rampelberg, B. D. Schutter, C. Detavenier, G. B. Marin, *Catal. Lett.* **2012**, *142*, 959–968.
[22] M. Arjmand, M. Keller, H. Leion, T. Mattisson, A. Lyngfelt, *Energy Fuels* **2012**, *26*, 6528–6539.
[23] M. J. Tiernan, P. A. Barnes, G. M. B. Parkes, *J. Phys. Chem. B* **1999**, *103*, 338–345.

[24] J. Y. Kim, J. A. Rodriguez, J. C. Hanson, A. I. Frenkel, P. L. Lee, *J. Am. Chem. Soc.* **2003**, *125*, 10684–10692.

[25] A. Pineau, N. Kanari, I. Gaballah, *Thermochim. Acta* **2006**, *447*, 89–100.

[26] D. Chadda, J. D. Ford, M. A. Fahim, *Int. J. Energy Res.* **1989**, *13*, 63–73.

[27] G. V. Malinin, Y. M. Tolmachev, *Russ. Chem. Rev.* **1975**, *44*, 392–397.

[28] A. Malecki, B. Prochowska-Klisch, *J. Therm. Anal.* **1994**, *41*, 1109–1117.

[29] M. Maciejewski, *J. Therm. Anal.* **1992**, *38*, 51–70.

[30] S. Vyazovkin, *Thermochim. Acta* **2003**, *397*, 269–271.

[31] L. H. Yue, M. Shui, Z. D. Xu, *Thermochim. Acta* **1999**, *335*, 121–126.

[32] P. X. Song, D. S. Wen, Z. X. Guo, T. Korakianitis, *Phys. Chem. Chem. Phys.* **2008**, *10*, 5057–5065.

[33] A. Navrotsky, C. C. Ma, K. Lilova, N. Birkner, *Science* **2010**, *330*, 199–201.

[34] A. Navrotsky, *ChemPhysChem* **2011**, *12*, 2207–2215.

[35] N. W. Piekiel, R. E. Cavicchi, M. R. Zachariah, *Thermochim. Acta* **2011**, *521*, 125–129.

[36] Y. Choi, M. Jung, Y. K. Lee, *Electrochem. Solid-State Lett.* **2009**, *12*, F17–F19.

[37] C. Fushimi, K. Araki, Y. Yamaguchi, A. Tsutsumi, *Ind. Eng. Chem. Res.* **2003**, *42*, 3922–3928.

[38] D. T. Y. Chen, *J. Therm. Anal.* **1975**, *7*, 61–64.

[39] A. K. Galwey, M. E. Brown, *Thermal Decomposition of Ionic Solids, Chemical Properties and Reactivities of Ionic Crystalline Phases, Vol. 86, 1st ed.*, Elsevier Science, New York, **1999**.

[40] W. Bergermayer, H. Schweiger, E. Wimmer, *Phys. Rev. B* **2004**, *69*, 195409.

[41] J. Li, S. Q. Wang, J. W. Mayer, K. N. Tu, *Phys. Rev. B* **1989**, *39*, 12367–12372.

[42] J. Li, J. W. Mayer, *Mater. Chem. Phys.* **1992**, *32*, 1–24.

[43] K. T. Sullivan, N. W. Piekiel, C. Wu, S. Chowdhury, S. T. Kelly, T. C. Hufnagel, K. Fezzaa, M. R. Zachariah, *Combust. Flame* **2012**, *159*, 2–15.

[44] F. Perinet, J. L. Duigou, C. Monty in *Non-Stoichiometric Compounds Surfaces, Grain Boundaries and Structural Defects, Vol. 276* (Eds.: J. Nowotny, W. Weppner), Kluwer Academic, Boston, **1989**, pp. 387–397.

[45] W. J. Moore, B. Selikson, *J. Chem. Phys.* **1951**, *19*, 1539–1543.

[46] C. G. Hill, *An Introduction to Chemical Engineering Kinetics and Reactor Design, 1st ed.*, Wiley, New York, **1977**, pp. 438–452.

[47] *Diffusion in Condensed Matter: Methods, Materials, Models* (Eds.: P. Heitjans, J. Karger), Springer Verlag, Berlin, **2005**, p. 344.

[48] P. R. N. Childs, *Practical Temperature Measurement*, Butterworth-Heinemann, London, **2001**, pp. 146–172.

[49] P. Saunders, D. R. White, *Metrologia* **2003**, *40*, 195–203.

[50] T. S. Ward, M. A. Trunov, M. Schoenitz, E. L. Dreizin, *Int. J. Heat Mass Transfer* **2006**, *49*, 4943–4954.

[51] S. Chowdhury, K. Sullivan, N. Piekiel, L. Zhou, M. R. Zachariah, *J. Phys. Chem. C* **2010**, *114*, 9191–9195.